scientific reports

Check for updates

OPEN

Fabrication of the magnetic mesoporous silica Fe-MCM-41-A as efficient adsorbent: performance, kinetics and mechanism

Yige Guo[1], Bin Chen[2]✉, Ying Zhao[3] & Tianxue Yang[3]✉

Antibiotics are emerging pollutants and increasingly present in aquaculture and industrial wastewater. Due to their impact on the environment and health, their removal has recently become a significant concern. In this investigation, we synthesized nano zero-valent iron-loaded magnetic mesoporous silica (Fe-MCM-41-A) via precipitation and applied the adsorption of oxytetracycline (OTC) from an aqueous solution. The effects of competing ions such as Na^+, Ca^{2+} and Cu^{2+} on the adsorption process under different pH conditions were studied in depth to providing a theoretical basis for the application of nanomaterials. The characterization of the obtained material through transmission electron microscopy demonstrates that the adsorbent possesses hexagonal channels, which facilitate mass transfer during adsorption. The loaded zero-valent iron made the magnetic, and was thus separated under an applied magnetic field. The adsorption of OTC onto Fe-MCM-41-A is rapid and obeys the pseudo-second-order kinetic model, and the maximum adsorption capacity of OTC is 625.90 mg g^{-1}. The reaction between OTC and Fe-MCM-41-A was inner complexation and was less affected by the Na^+. The effect of Ca^{2+} on the adsorption was small under acidic and neutral conditions. However, the promotion effect of Ca^{2+} increased by the increase of pH. Cu^{2+} decreased the removal efficiencies continuously and the inhibitory effects decrease varied with the increase of pH. We propose that surface complexing, ion-exchange, cationic π-bonding, hydrogen bonding, and hydrophobicity are responsible for the adsorption of OTC onto Fe-MCM-41-A.

Water is our most necessary resource. It is also becoming a scarce resource in many parts of the world. The pollutants in our water are also becoming more difficult to remove. Levels and kinds of antibiotics in our drinking water are all on the rise[1]. Oxytetracycline (OTC), as a broad-spectrum antibiotic, is extensively used in human therapy, livestock breeding and aquaculture[2,3]. Recent studies indicate that the OTC is roughly 100–340 ng L^{-1} in surface water[4,5], for example, the maximum detected and mean concentrations of oxytetracycline in Honghu lake, China are up to 2796.6 and 161.9 ng L^{-1} [6]. The continuous presence of OTC in environment can harm the growth of plants and animals and cause resistance genes[7].

Oxytetracycline (OTC) is difficult to degrade owing to its toxicity and resistance to microorganism[8]. The elimination of OTC in few of the biological treatments has been distinguished by quick sorption and slow biodegradation[9]. Traditional water treatment technologies have a limited removal efficiency of 20–30% for antibiotics[10]. Besides, antibiotic pollution is characterized by pH dependence and heavy metal contamination[11]. OTC is a complex organic compound and show positive, zwitterion or negative charges vary with pH. The active groups of OTC will combine with metal ions to form complex pollutants, which will affect each other's characteristics and enhance toxic effects[12]. Therefore, the demand for effective removal of OTC is urgent.

Treatment techniques based on physical and chemical methods, such as adsorption, are the forefront of water remediation[13]. In the past few decades, the emergence of nanomaterials has greatly promoted the development of water treatment technology[14,15]. MCM-41 is a silica-based material which can be adopted as an adsorbent owing

[1]College of Geology and Environment, Xi'an University of Science and Technology, Xi'an 710054, China. [2]Shaanxi Provincial Center for Disease Control and Prevention, Xi'an 710054, China. [3]State Key Laboratory of Environmental Criteria and Risk Assessment, Chinese Research Academy of Environmental Sciences, Beijing 100012, China. ✉email: chenbin6121@163.com; 2316378041@qq.com

to its larger surface area, flexible pore structure, larger pore volume, and nontoxicity[16]. The hexagonal phase channel expedites the adsorption of oxytetracycline, a polycyclic macromolecule. The nanoscale pore channels inside the material can provide a large number of adsorption reaction micro-interfaces, which can change the material and energy transfer process on the interface, promote concentration accumulation of pollutants, reaction activation, and advance the reaction[17].

The MCM-41 has been assembled with zeolites (e.g., zeolite A, zeolite X), iron oxide nanoparticles and et al. to enhance its performance[18–20]. Nanoscale zero-valent iron (NZVI) has recently drawn rising attention for water pollution remediation due to its high activity and separability[21]. However, to the best of the author's knowledge, little information has been reported on the performance and mechanism of removal of OTC from water using NZVI-loaded MCM-41-zeolite composites, which is the objective of this investigation.

Herein, an efficient method was developed for the remediation of OTC. The specific objectives were (1) to synthesize and characterize nano zero-valent iron (NZVI)-loaded magnetic mesoporous silica (Fe-MCM-41-A); (2) to examine OTC removal performance under different conditions, i.e., initial solution pH initial concentrations, adsorbent dosages and competition ions; (3) to carry out the adsorption kinetics and thermodynamics analysis; and (4) to elucidate the possible adsorption mechanisms for the removal of OTC.

Materials and methods

Materials. OTC (> 97% purity), $Na_2O_3Si{\cdot}9H_2O$ (AR), $NaAlO_2$ (AR) were obtained from Shanghai Minrell Chemical Technology Co., LTD. NaOH (AR), $NaBH_4$ (> 98% purity), $C_{19}H_{42}BrN$ ((CTAB) AR), $FeCl_3$ $6H_2O$ (AR), NaCl (AR), $CaCl_2$ (AR), $CuCl_2$ (AR), HCl (99 wt.%), $C_2H_2O_4$ (AR), C_2H_5OH (AR), C_2H_3N (GR) and HNO_3 (AR) were supplied by Sinopharm Chemical Reagent Co., Ltd (China). Deionized water was used in all experiments.

Preparation of Fe-MCM-41-A. We synthesized MCM-41-A through impregnation-assisted one-step crystallization method[22]. The specific preparation process was described in the Supplementary information. Fe-MCM-41-A and NZVI were synthesized according to the previously reported precipitation method[8]. MCM-41-A (4.0 g) and $FeCl_3.6H_2O$ (19.32 g) were dispersed in 100 mL degassed C_2H_5OH solution (80 wt%) after 30 min of magnetically stirring 200 mL of 1 M $NaBH_4$ (approximately 4–5 mL min^{-1}) was added dropwise under stirring. All procedures were conducted under N_2 environment. The obtained solid suspension was rinsed more than three times with ethanol, then drying to constant weight under vacuum condition at 50 °C. NZVI was synthesized by the above steps without MCM-41-A.

Adsorbents characterization. The morphology of Fe-MCM-41-A was observed by TEM (Tecnai G2 F20). The BET measurements and pore-size distribution were performed (Specific Surface Area Analyzers), the crystal structure of Fe-MCM-41-A was characterized by XRD (Ulitma IV), UV–Vis DRS, FT-IR (TENSOR 37), XPS (Axis Ultra DLD), Mossbauer analysis and magnetization analyses were further employed to characterize the obtained samples.

Batch experiments. *Adsorption efficiency experiments.* The adsorption efficiency experiment was carried out by single factor experiment[8]. Adsorption studies were conducted at different contact times, pH, and initial concentrations to assess the potential removal of OTC. Moreover, the adsorption mechanisms have been presented based on the achieved results. The specific experimental steps were described in the Supplementary information.

Competitive ion experiments. A gradient series of concentrations of Na^+ or Ca^{2+} solutions (0.01, 0.02, 0.05, 0.1 M) and Cu^{2+} solutions (5.0, 10.0, 20.0 and 50.0 mg L^{-1}) were prepared and used as background solutions to obtain OTC solution. The other steps are the same as the adsorption efficiency experiments as showed in Supplementary information. Computational details were described in the Supplementary information.

Regeneration experiments. The exhausted Fe-MCM-41-A was regenerated by Ultrasonic reduction method. The OTC was desorbed through ultrasonic method and the reactivity of Fe-MCM-41-A was recovered by reduction of sodium borohydride. The specific experimental steps were described in the Supplementary information.

Results and discussion

Characterization of Fe-MCM-41-A. The SEM image and EDX of Fe-MCM-41-A showed in Fig. 1a,b demonstrates the linear nano-structure of the material and that the sample has loose texture and uniform structure. According to the HRTEM and TEM images (Fig. 1d,e), it can be seen that the sample exhibited a hexagonal pore structure and Fe^0 is uniformly loaded in the sample. These results demonstrate that the mesopore structure was not undermined by Fe loading. Figure 1d shows that the sample has an ordered arrangement of hexagonal channels with uniform pore size of 3.4 nm. This indicates that the material keeps the pore structure well after the loaded of zero-valent iron. This mesoporous structure of the material is conducive to the mass transfer process of the adsorption reaction and the increase of the adsorption capacity.

As indicated in Fig. 1S, the surface area and average pore size of Fe-MCM-41-A is 360.4 m^2 g^{-1} and 3.4 nm, respectively, which is consistent with the analysis of TEM. The small angle (0.7°–10°) XRD analysis of Fe-MCM-41-A (Fig. 2S) show the characteristic diffraction peaks at 2θ of 2.1° and 4.2° represent the (110) and (200), planes of Fe-MCM-41-A with hexagonal mesoporous crystal structure, respectively[23]. The 2θ peak at 44.9° designates

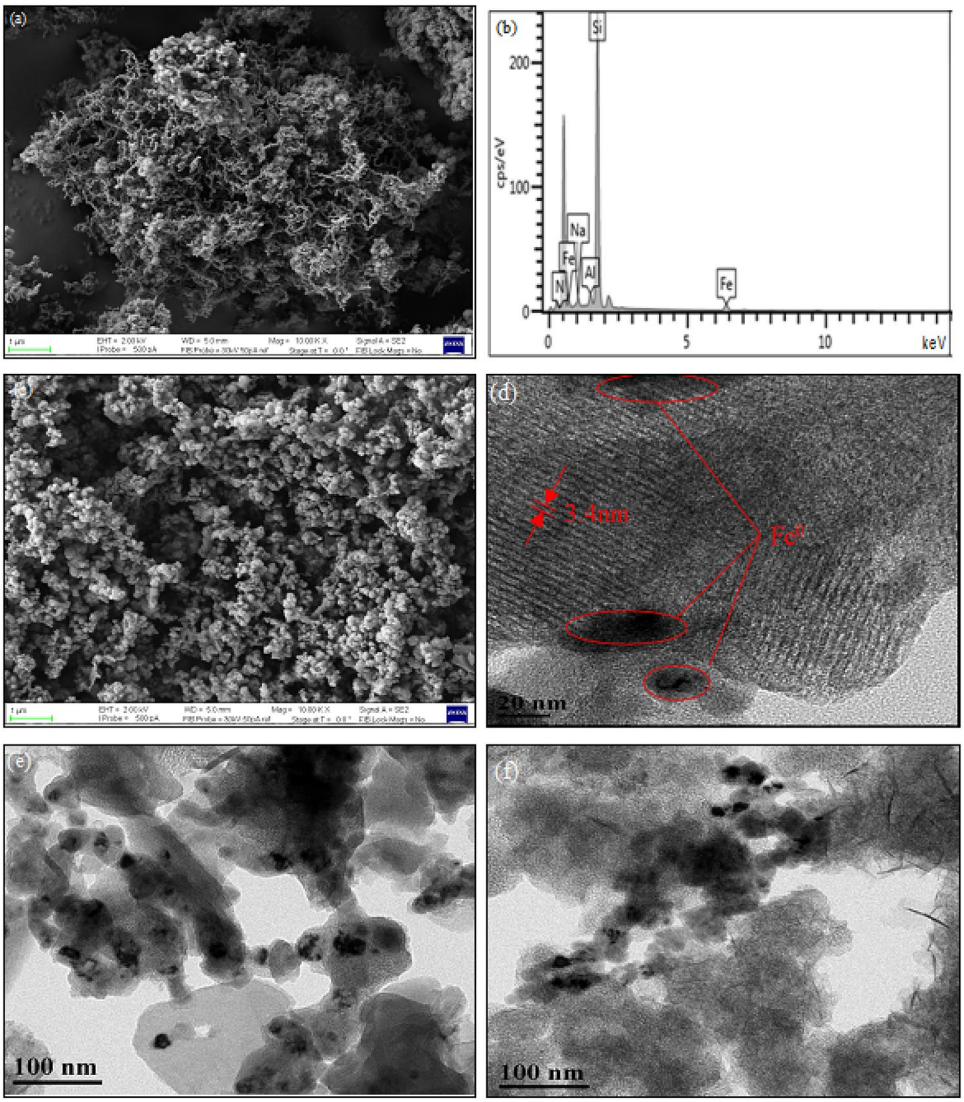

Figure 1. (**a**) SEM and (**b**) EDX of Fe-MCM-41-A, (**c**) SEM of OTC-Fe-MCM-41-A, (**d**) HRTEM of Fe-MCM-41-A, (**e**) TEM of Fe-MCM-41-A and (**f**) OTC-Fe-MCM-41-A.

that Fe in the material is mainly zero-valent[24]. The small peak at 37° represents iron oxidation which may be due to the oxidation of Fe0 during preservation.

It can be seen from Fig. 2b that the characteristic peak of Al in Fe-MCM-41-A decreases significantly, while the characteristic peak of Fe in Fe-MCM-41-A increases accordingly. This demonstrated that the content of Al in MCM-41-A decreases and the content of Fe element increases after the loading modification of NZVI. It can be seen from Fig. 2d that photoelectron peaks appear in the Fe 2p3/2 spectra. The peak of 707.1 eV corresponds to the fe2p3/2 electron orbital peak of Fe^0[25], indicated that the sample in freshly synthesized contains zero valent iron. This analysis is consistent with the XRD analysis. So, we speculated that a decrease in the Al content of Fe-MCM-41-A during modification may be due to the replacement of Fe in the skeleton of MCM-41-A[26].

To further investigate the nature and binding form of Fe in Fe-MCM-41-A, DRS UV–Vis spectroscopy experiments were conducted and the results are shown in Fig. 3. Silicon based multihole materials have no bands in 200–270 nm region[27] and the absorption bands at 287 nm may be contributed by the pore structure of Fe-MCM-41-A[28]. However, the sample shows absorption bands centered at 210–250 nm, this indicates that Fe has been dispersed within the material. The bands at 211 nm and 248 nm may be assigned to the d¼–p¼ charge-transfer transition between the iron and oxygen atoms in the framework of Fe–O–Si in Fe-MCM-41-A[29]. So, we assume that the schematic diagram of displacement reaction in the modification process as shown in Fig. 4.

Figure 5 shows the Mössbauer spectrum of Fe-MCM-41-A, and this spectrum is a superposition of one major paramagnetic doublet and one minor broad magnetic sextet. The six-line pattern of the spectrum is characteristic of the body-centered cubic face of metallic α-Fe confirmed by the hyperfine interaction parameter values shown in Table 1. The major paramagnetic doublet indicating that the paramagnetic state of the sample[30], therefore, the agglomeration of Fe-MCM-41-A caused by excessive residual magnetism can be avoided. The small contribution

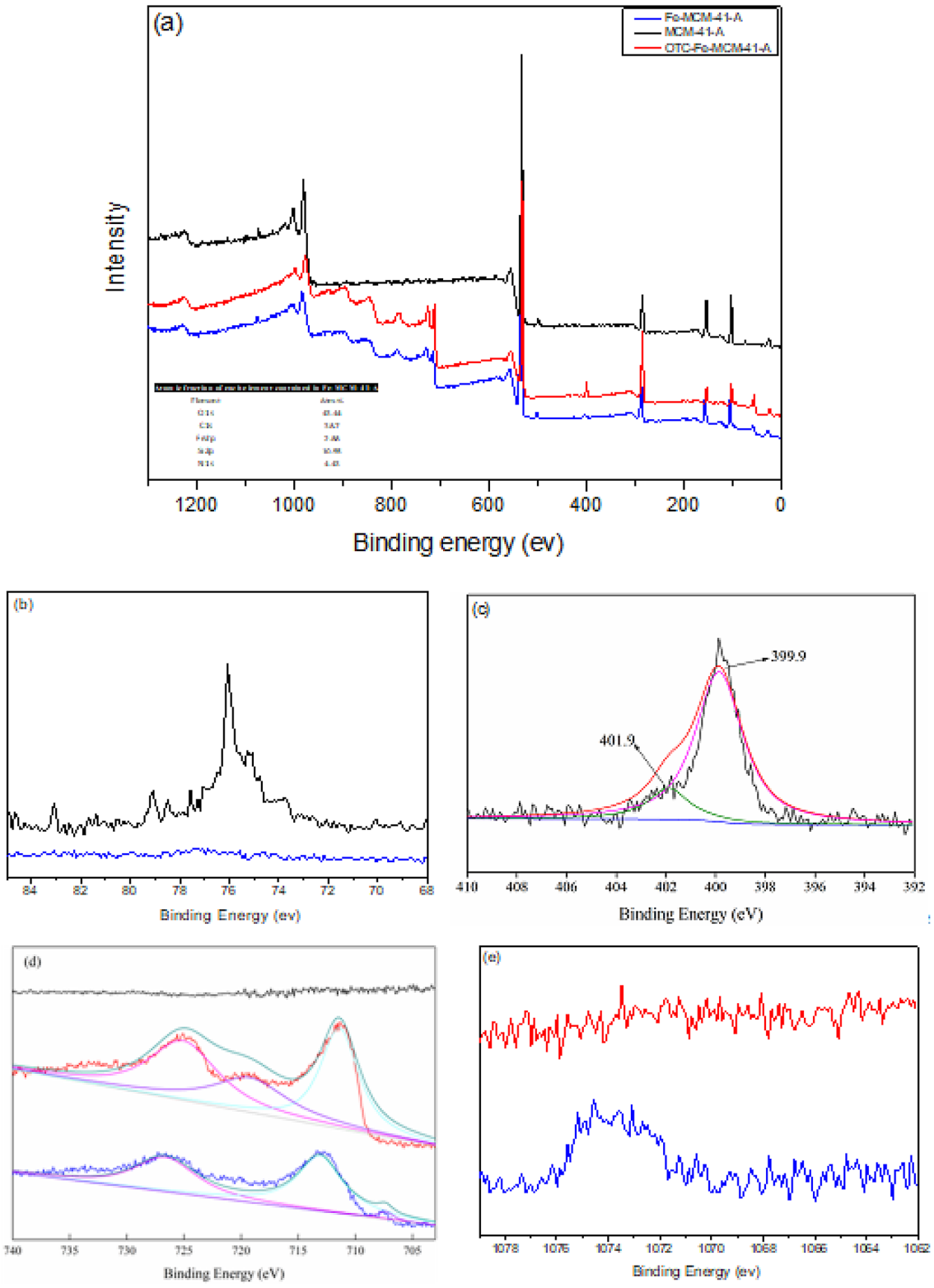

Figure 2. (**a**) Full survey XPS spectra of MCM-41-A, Fe-MCM-41-A and OTC-Fe-MCM-41-A. The XPS spectra of (**b**) Al in MCM-41-A and Fe-MCM-41-A, (**c**) N1s in OTC-Fe-MCM-41-A, (**d**) Fe2p in MCM-41-A, Fe-MCM-41-A and OTC-Fe-MCM-41-A, (**e**) Na in Fe-MCM-41-A and OTC-Fe-MCM-41-A.

of the sextet may be due to refinements of the structure to the nanometer level of Fe. As shown in Table 1, the doublet (IS of 0.33 mm/s and QS of 0.76 mm/s) indicates the positively charged Fe in the sample[31], the sextet

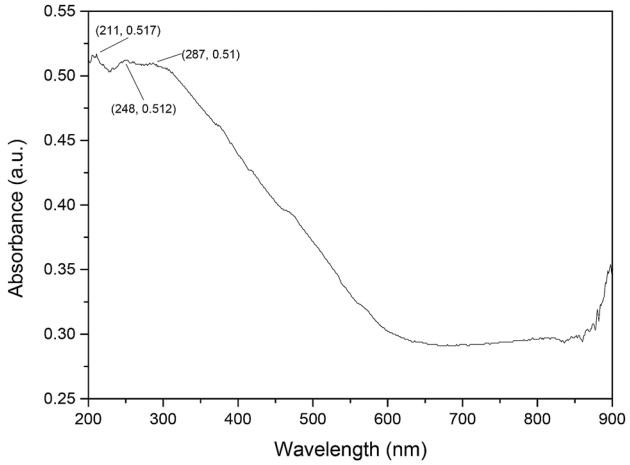

Figure 3. UV–Vis DRS spectrum of Fe-MCM-41-A.

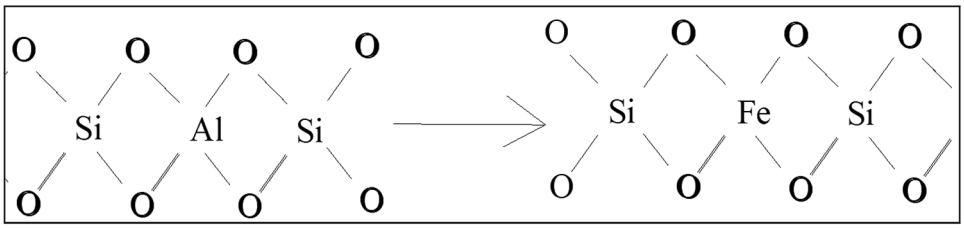

Figure 4. The replacement of Fe in cage construction of Fe-MCM-41-A.

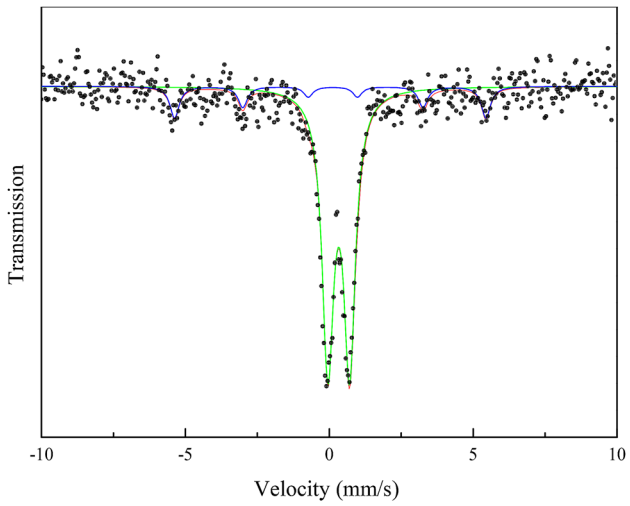

Figure 5. Mossbauer spectrum of Fe-MCM-41-A at room temperature.

Component/compound	IS(mm s^{-1})	QS (mm s^{-1})	B_{hf} (KOe)	Γ (mm s^{-1})
Sextet/iron	0.330 (11)	0.755 (19)	–	0.244 (14)
Doublet/sextetiron	0.081 (66)	– 0.046 (66)	335.5(45)	0.193 (98)

Table 1. Hyperfine interaction parameters of Fe-MCM-41-A measured by Mössbauer spectroscopy.

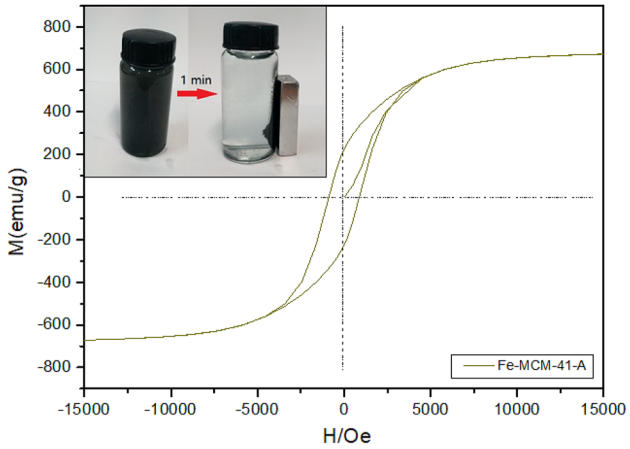

Figure 6. Hysteresis loop of Fe-MCM-41-A and separation effect applied magnetic field in 1 min.

(IS of 0.081 mm/s and QS of − 0.046 mm/s) indicates the existence of Fe0[32]. Since the sample was subjected to Mössbauer analysis more than 2 months after its preparation, the sample may be partially oxidized which is consistent with the XPS analysis.

Uncertainty of the values is given in parentheses for the last significant number. IS isomer shift relative to α-iron, QS quadrupole splitting for the doublet and quadrupole shift for the sextet, B_{hf} hyperfine magnetic field, Γ half width at half maximum of spectral lines.

The zero-valent iron loaded material is magnetic and can be separated quickly under applied magnetic field. The magnetization properties of Fe-MCM-41-A were analyzed by hysteresis loop test. Figure 6 shows that Fe-MCM-41-A is strongly magnetic and can be separated within 1 min under applied magnetic field.

Adsorption performance. *OTC removal efficiency using NZVI, MCM-41-A and Fe-MCM-41-A.* Comparison of NZVI, MCM-41-A and Fe-MCM-41-A in OTC removal was shown in Fig. 7a. The adsorption of OTC onto Fe-MCM-41-A and McM-41-a reach an equilibrium in 60 min, the OTC removal rate was 98.4% and 71.04%, respectively. However, the adsorption of OTC onto NZVI reached equilibrium in ~ 100–150 min, with a removal rate of 75.2%. The rapid adsorption of OTC onto Fe-MCM-41-A and MCM-41-A is mainly due to the cellular mesoporous structure that facilitates mass transfer[17,33], the large specific surface area and the charged surface of the material[34]. Moreover, the OTC removal rate of Fe-MCM-41-A is higher than that of MCM-41-A, indicating that modification of MCM-41-a by NZVI load is conducive to improving the adsorption performance.

Removal kinetics. The adsorption of OTC onto Fe-MCM-41-A is rapid especially in the first 20 min (Fig. 7a). This high adsorption was mainly due to the large surface area, hexagonal mesoporous structure and appropriate pore size of Fe-MCM-41-A which promote internal mass transfer during the adsorption[35]. In this work, the adsorption capacity of OTC was 196.8 mg g^{-1}, when 100 mg L^{-1} OTC solution was remediated with Fe-MCM-41-A (0.5 g L^{-1}) at pH 5.0. Correlation coefficient ($R^2 = 0.9999$) indicates that the adsorption obeys the pseudo-second-order kinetic model (Table 2). This indicates that the removal of OTC was rate-controlling limiting step.

Effect of pH. Figure 7b reveals that from pH 2.0 to 5.0, the removal efficiency increased from 92.2 to 98.4%, and then from pH 5.0 to 11.0, the efficiency decreased from 98.4 to 76.7%. This proves that a weak acidic condition could favor the adsorption process. The adsorption of OTC onto Fe-MCM-41-A reached equilibrium in 40 min at pH 4.0 and 5.0; however, the adsorption lasted for more than 150 min at pH 2.0 and 11.0. This could be due to the digestion of Fe and the desilication of Fe-MCM-41-A under strong acidic and alkaline conditions. The highest adsorption efficiency was achieved at pH 5.0. When the pH is higher than 7.4 (pK_{a2}), HL^- and L^{2-} become predominant species and Kow of OTC also decreases, thereby Fe-MCM-41-A surfaces become negative simultaneously. By this, we could infer that a decrease in the removal efficiency at pH 11.0 might be largely due to the weakening of hydrophobic function[35].

Effect of adsorbent dosage. Figure 7c exhibits that the removal efficiency of OTC increased with the amount of adsorbent. When the dosage reached 0.5 g L^{-1}, the removal efficiency no longer increased with the amount of adsorbent owing to agglomeration and particle precipitation of Fe-MCM-41-A at high solid to liquid ratio.

Effect of initial OTC concentration. It has been noticed that the initial concentration of OTC can significantly influence the removal efficiency. Figure 7d shows that the adsorption capacity of OTC increased and the removal efficiency increased at first and then decreased with an increase in the initial concentration. The highest removal efficiency was 99.1% at an initial concentration of 50 mg L^{-1}, and the maximum equilibrium adsorption capacity was 609.0 mg g^{-1} at an initial concentration of 500 mg L^{-1}. The main reason for the decrease of adsorption efficiency was the lack of adsorption sites. The enhancement of the adsorption capacity was due to the high driving

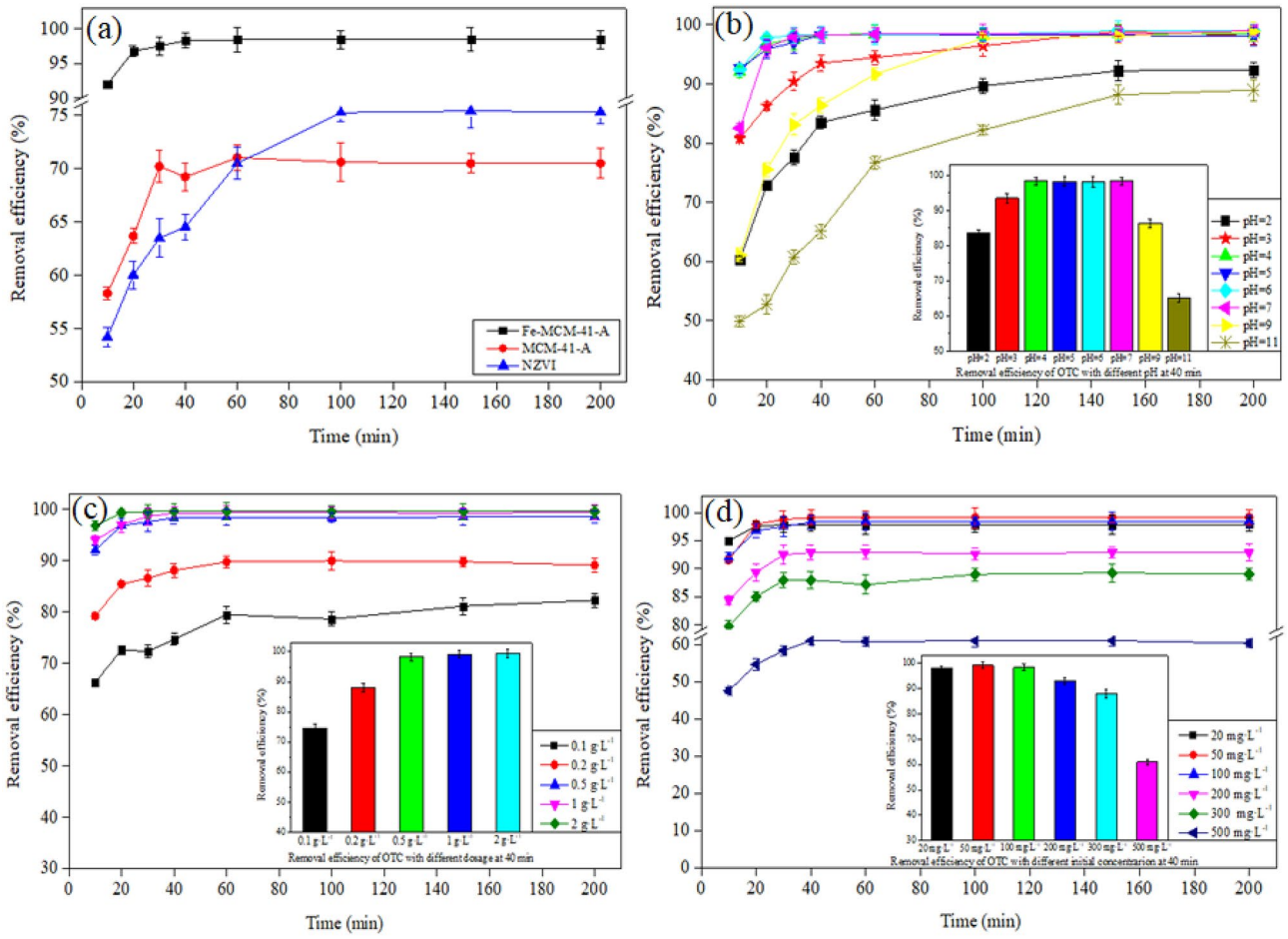

Figure 7. (**a**) Comparison of NZVI, MCM-41-A and Fe-MCM-41-A in OTC removal, C_0: 100 mg L^{-1}; dosage: 0.5 g L^{-1}; T: 25 °C. Removal efficiency of OTC onto Fe-MCM-41-A in different conditions: (**b**) C_0: 100 mg L^{-1}; dosage: 0.5 g L^{-1}; T: 25 °C, (**c**) C_0: 100 mg L^{-1}; pH 5.0; T: 25 °C, (**d**) dosage: 0.5 g L^{-1}; pH 5.0; T: 25 °C.

Kinetic model	Equation	Parameters	Value
Pseudo-first-order	$\log(q_e - q_t) = \log q_e - k_1/2.303t$	k_1 (min^{-1})	0.1011
		q_e (mg g^{-1})	30.49
		R^2	0.9792
Pseudo-second-order	$(t/q_t) = 1/(k_2 q_e) + 1/q_e(t)$	k_2 (g mg^{-1} min^{-1})	1.6531
		q_e (mg g^{-1})	197.94
		R^2	0.9998

Table 2. Parameters in adsorption kinetic equation of OTC onto Fe-MCM-41-A.

force caused by the high concentration gradient. Besides, at high initial OTC concentrations, a large number of OTC were distributed around Fe-MCM-41-A, complex $[Fe(TC)]_n^{3+}$ were formed and deposited on the surface of the adsorbent instantaneously, thus might block the mass transfer channels[36]. The higher initial OTC concentration led to faster formation of $[Fe(TC)]_n^{3+}$, hence, the longer reaction equilibrium time.

Effect of ions. Figure 8 shows that the removal efficiency of OTC reduced less than 7% while the concentration of Na^+ in background solution increased from 0.0 M to 0.1 M in each pH condition. The adsorption was less affected by the Na^+, this was owing to the inner complexation between OTC and Fe-MCM-41-A[37], as inner layer complexation can be hardly affected by the ionic strength in the background solution[38,39].

Figure 8 shows that the effect of Ca^{2+} on the adsorption was small under acidic and neutral conditions. However, the removal efficiency increased with the increasing of the concentration of Ca^{2+} under alkaline condition, and the promotion effect increased by the increase of pH. This was mainly benefit from the bridging effect of Ca^{2+}, OTC combined with Ca^{2+} to form TCs-Ca^{2+}-Fe-MCM-41-A[40].

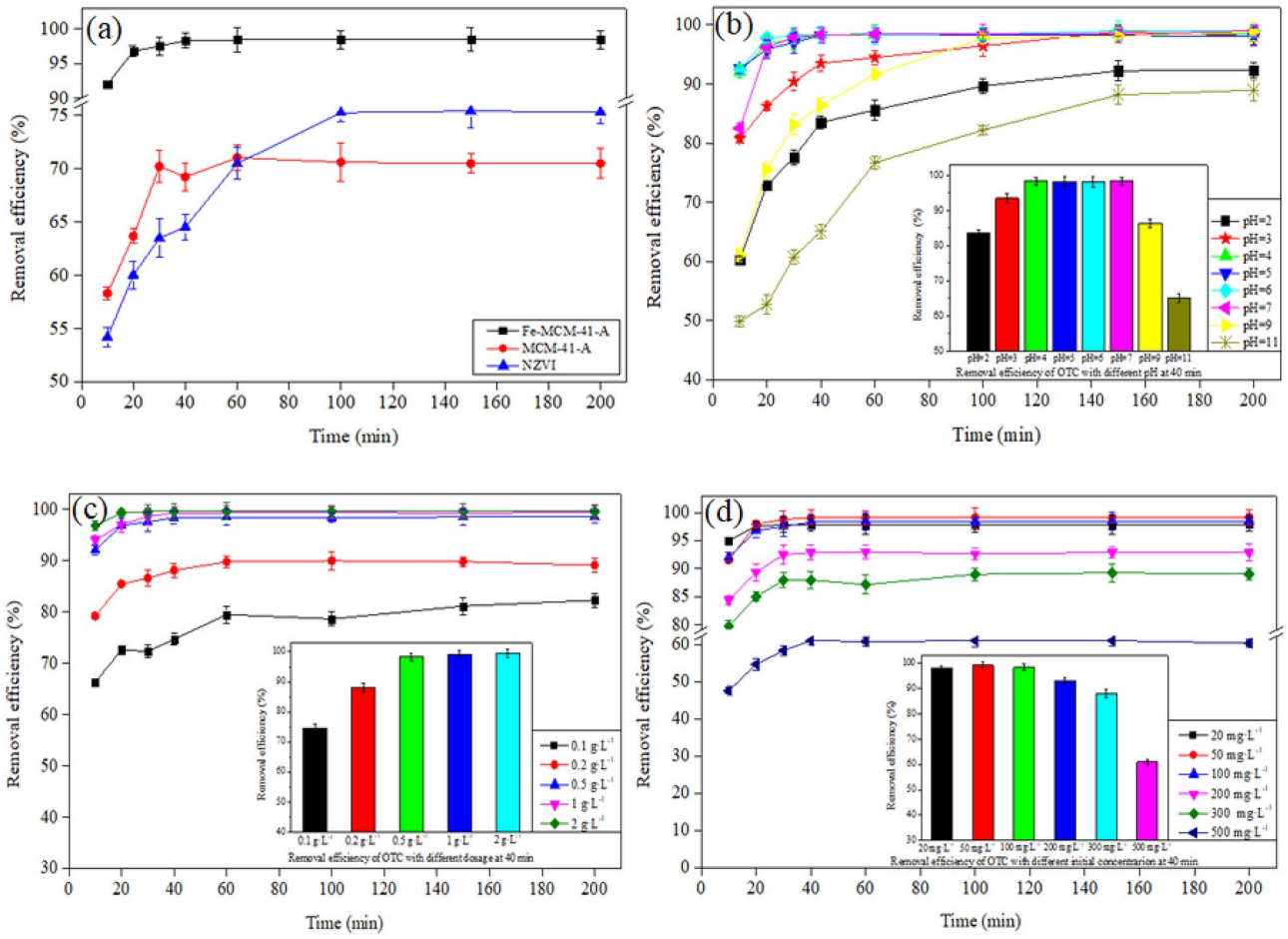

Figure 8. Effects of ionic strength on the removal efficiency of OTC onto Fe-MCM-41-A under varied pH (**a**) Na^+, (**b**) Ca^{2+}, (**c**) Cu^{2+} and (**d**) removal efficiency of Cu^{2+}.

Another reason for the removal efficiency of TCs increased with the increasing of Ca^{2+} concentration under alkaline condition was the effect of surface chemical precipitation. TCs molecules may complex with Ca^{2+} and deposited on the surface of Fe-MCM-41-A[41]. Besides Ca^{2+} could reduce the hydrophilicity of OTC and helped to prompt TCs adsorbed onto Fe-MCM-41-A under hydrophobic forces[42].

The removal efficiencies of TCs onto Fe-MCM-41-A decreased continuously with the increase of Cu^{2+} (Fig. 8), meanwhile, the inhibitory effects of Cu^{2+} decrease varied with the increase of pH. The inhibiting effect of Cu^{2+} was mainly due to the complexation between Cu^{2+} and TCs. The surface charge of OTC increased after complexation with Cu^{2+} and the electrostatic repulsion between OTC and Fe-MCM-41-A also increased, which may inhibit the removal of OTC.

Adsorption isotherm. According to the adsorption isotherms analysis on the removal of OTC, we found that the equilibrium concentration increased along with the amount of OTC adsorbed onto Fe-MCM-41-A. The adsorption of OTC onto Fe-MCM-41-A obeys the Langmuir model (Table 3). The constant q_{max} at 25 °C obtained from Langmuir model was 625.90 mg g^{-1}. This indicates that the adsorption of OTC onto Fe-MCM-41-A follows monolayer adsorption which occurs on a relatively uniform surface.

Adsorption mechanism. The functional groups of Fe-MCM-41-A, OTC-Fe-MCM-41-A and OTC were measured by FT-IR. As shown in Fig. 9, the characteristic peaks of OTC are principally placed at 1200–1700 cm^{-1}. Peaks at 1615 cm^{-1}, 1587 cm^{-1},1458 cm^{-1} and 1366 cm^{-1} can be attributed to attributed to a stretching of the C=O groups, C–H bonds, amide-NH groups and C–N bonds, respectively[43,44]. The typical bands of C–N and amide-NH shifted to higher frequencies after adsorption, indicating the reaction between amide groups in OTC with Fe-MCM-41-A. The peak located in 3200–3500 cm^{-1} can be assigned to –OH band. The broadening and peak of –OH band strength weakening after the adsorption, indicated that the –OH band in OTC changed from free state to association state[45]. This may be due to the hydrogen bonding between neutral -OH band and non-ionized –Si–OH band in TCs[46].

XPS were further employed to study the adsorption mechanism (Fig. 2), the results of analysis prove that the intensities of N 1s increased, whereas the intensities of Na 1s decreased after adsorption. This could be due to that parts of OTC adsorb onto Fe-MCM-41-A through ion-exchange. In Fig. 2c the peaks at 399.9 eV and 401.9 eV

Adsorption isotherm model	Equation	Parameters	Value
Langmuir	$\frac{C_e}{q_e} = \frac{1}{q_{max}k} + \frac{1}{q_{max}}C_e$	k (L mg^{-1})	0.1758
		Q_{max} (mg g^{-1})	625.90
		R_L	0.0538
		R^2	0.9989
Freundlich	$\log q_e = \log K_f + \frac{1}{n}\log C_e$	K_f (mg g^{-1})	107.4484
		1/n	0.3929
		R^2	0.8485

Table 3. Isotherm constant parameters and R^2 calculated for the adsorption of OTC onto Fe-MCM-41-A.

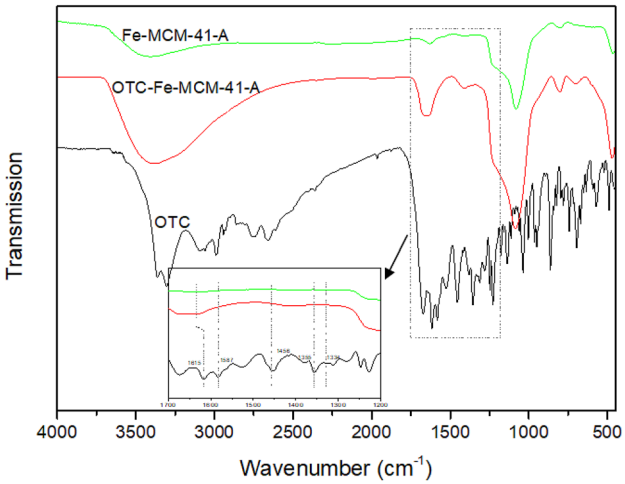

Figure 9. FT-IR spectrograms of Fe-MCM-41-A, OTC-Fe-MCM-41-A and OTC.

could be correspond to the amino group and its disturbation caused by Fe after adsorption, respectively, indicated that Fe-MCM-41-A could be combined with the amino bands in OTC by cationic—bonding. The $Fe2p_{3/2}$ and $Fe2p_{1/2}$ spectra emerged at the binding energies of 725.2 eV and 711.4 eV, respectively, the chemical shift in the spin–orbit coupling was 13.8 eV (Fig. 2d). This suggests that the cationic-bond between Fe-MCM-41-A and -NH on OTC could be formed through polarization[47].

Besides, according to the law of removal efficiency and octanol–water distribution coefficient (Kow) of OTC, it can be inferred that an increase in the hydrophobicity of OTC is conducive to the adsorption of OTC on Fe-MCM-41-A.

Comparison of various adsorbent. Performances of different materials for the adsorption of OTC were compared in Table 4. The q_{max} of OTC onto Fe-MCM-41-A was higher than other similar materials. This honeycomb-like magnetic mesoporous silica Fe-MCM-41-A synthesized in this study was superior to other materials in both adsorption rate and efficiency.

Regeneration of Fe-MCM-41-A. In the regeneration experiment, the removal rate remained above 78% (Fig. 10) after five rounds of sorption–desorption cycles, indicating that Fe-MCM-41-A has a good regenerability. From Fig. 1c and f it can be seen that after the adsorption of OTC the adsorbent retains the original morphology and pore structure well, which also proves that the structural stable material is renewable. Leaching of iron was investigated after each cycle as an indication of the stability of Fe-MCM-41-A. As shown in Fig. 10, the amount of leached iron ions was the highest in the first cycle (0.87 mg L^{-1}). After third cycle, leached iron reduced to < 0.09 mg L^{-1} and reasonably stable for the subsequent cycles reducing to 0.05 mg L^{-1} at the fifth cycle. The change law of iron loss is consistent with that of adsorbent regeneration property, so we assumed that this trivial iron loss is an important factor for reuse of the adsorbent. The decrease in removal efficiency occurred mainly in the second cycle, this might have been caused by an irreversible occupation of partial-adsorption sites and the loss of nano-absorbent, as has been observed in previous studies[8].

Conclusions

A kind of magnetic hexagonal mesoporous silica Fe-MCM-41-A was synthesized and demonstrated to be an efficient adsorbent for the removal of OTC from aqueous solution. The ordered hexagonal pore structure of Fe-MCM-41-A which can facilitate mass transfer was observed by TEM and XRD analysis. The adsorption

Adsorbate	Adsorbent	Time (h)	Dosage (g L^{-1})	pH	T (°C)	q_{max} (mg g^{-1})	References
OTC	Undecenoic acid-coated MNPs	–	–	5.0	15	86.96	[48]
	MIL-101(HCl)	1	–	–	25	44.7	[49]
		1	–	–	5	115.34	[49]
	Activated sludge	–	–	5	20	90.9	[50]
	Activated carbon Sorbo Norit	192	1	4–5	25	252.6	[51]
	Activated carbon Merck	192	1	4–5	25	413.2	[52]
	Cyclodextrin Polymer	0.5	20	4–7	25	1.2	[53]
	MWCNT	100	–	7	23	73	[54]
	Fe-MCM-41-A	1	0.5	5	25	625.9	This work

Table 4. Comparison of removal capacities of OTC with various materials.

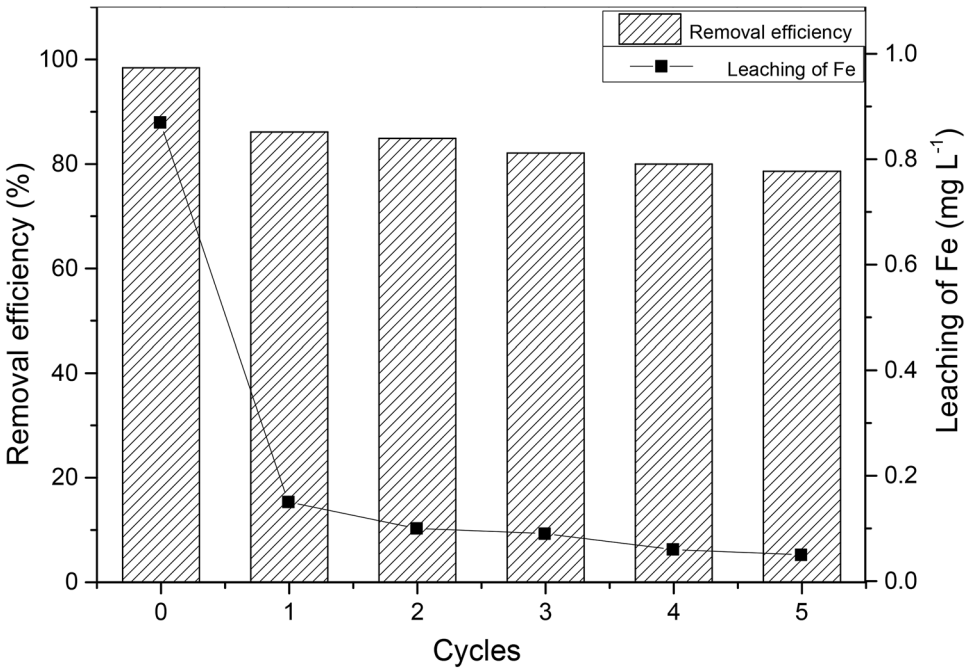

Figure 10. Removal efficiency of Fe-MCM-41-A after repeated regeneration and iron leaching after repeated regeneration for five cycles (pH 5.0, C_0: 100 mg L^{-1}; dosage: 0.5 g L^{-1}; T: 25 °C).

of OTC onto Fe-MCM-41-A is rapid and obeys the pseudo-second-order kinetic model. The obtained value of q_{max} according to Langmuir model was 625.90 mg g^{-1}. We propose that surface complexing, ion-exchange, cationic π-bonding, hydrogen bonding, and hydrophobicity are responsible for the adsorption of OTC onto Fe-MCM-41-A.

Data availability

The datasets generated during and/or analysed during the current study are available from the corresponding authors on reasonable request.

Received: 11 September 2020; Accepted: 6 January 2021
Published online: 28 January 2021

References

1. Mohan Sharma, B. *et al.* Health and ecological risk assessment of emerging contaminants (pharmaceuticals, personal care products, and artificial sweeteners) in surface and groundwater (drinking water) in the Ganges River Basin, India. *Sci. Total Environ.* **646**, 1459–1467 (2019).
2. Liu, J., Zhou, D., Xu, Z. & Zheng, S. Adsorptive removal of pharmaceutical antibiotics from aqueous solution by porous covalent triazine frameworks. *Environ. Pollut.* **226**, 379–384 (2017).
3. Adhikari, S., Selvaraj, S. & Kim, D.-H. Construction of heterojunction photoelectrode via atomic layer deposition of Fe_2O_3 on Bi_2WO_6 for highly efficient photoelectron chemical sensing and degradation of tetracycline. *Appl. Catal. B Environ.* **244**, 11–24 (2019).

4. Watkinson, A. J. The occurrence of antibiotics in an urban watershed: from wastewater to drinking water. *Sci. Total Environ.* **407**, 2711–2723 (2009).
5. Kolpin, D. W., Skopec, M., Meyer, M. T., Furlong, E. T. & Zaugg, S. D. Urban contribution of pharmaceuticals and other organic wastewater contaminants to streams during differing flow conditions. *Sci. Total Environ.* **328**, 119–130 (2004).
6. Wang, Z. *et al.* Occurrence and ecological hazard assessment of selected antibiotics in the surface waters in and around Lake Honghu, China. *Sci. Total Environ.* **609**, 1423–1432 (2017).
7. Adegoke, A. A., Faleye, A. C., Singh, G. & Stenstroem, T. A. Antibiotic resistant superbugs: assessment of the interrelationship of occurrence in clinical settings and environmental niches. *Molecules* **29**, 1–17 (2017).
8. Guo, Y. G. *et al.* Removal of tetracycline from aqueous solution by MCM-41-zeolite A loaded nano zero valent iron: synthesis, characteristic, adsorption performance and mechanism. *J. Hazard Mater.* **339**, 22–32 (2017).
9. Shi, Y., Wang, X. & Qi, Z. Sorption and biodegradation of tetracycline by granules and the toxicity of tetracycline on granules. *J. Hazard Mater.* **191**, 103–109 (2011).
10. Zhang, Q. Q., Ying, G. G., Pan, C. G., Liu, Y.-S. & Zhao, J.-L. Comprehensive evaluation of antibiotics emission and fate in the River Basins of China: source analysis, multimedia modeling, and linkage to bacterial resistance. *Environ. Sci. Technol.* **49**, 6772–6782 (2015).
11. Tian, Q. *et al.* Characterization of a robust cold-adapted and thermostable laccase from Pycnoporus sp. SYBC-L10 with a strong ability for the degradation of tetracycline and oxytetracycline by laccase-mediated oxidation. *J. Hazard Mater.* **382**, 121084. https://doi.org/10.1016/j.jhazmat.2019.121084 (2020).
12. Nguyen, C. C., Hugie, C. N., Kile, M. L. & Navab Daneshmand, T. Association between heavy metals and antibiotic-resistant human pathogens in environmental reservoirs: a review. *Front. Environ. Sci. Eng.* **13**, 46–63 (2019).
13. Jiuhui, Qu. *et al.* Critical fundamental scientific problems in reclamation and reuse of municipal waste water. *China Basic Sci.* **1**, 6–12 (2017).
14. Homaeigohar, S. The nanosized dye adsorbents for water treatment. *Nanomaterials* **10**, 1–43 (2020).
15. Alam, S. *et al.* Iron oxide nanoparticles embedded onto 3D Mesochannels of KIT-6 with different pore diameters and their excellent magnetic properties. *Chem. Asian J.* **6**, 834–841 (2011).
16. Eimer, G. A., Pierella, L. B., Monti, G. A. & Anunziata, O. A. Synthesis and characterization of Al-MCM-41 and Al-MCM-48 mesoporous materials. *Catal. Lett.* **78**, 65–75 (2002).
17. Nair, R. R., Wu, H. A., Jayaram, P. N., Grigorieva, I. V. & Geim, A. K. Unimpeded permeation of water through on of water through helium-leak-tight graphene-based membranes. *Science* **335**, 442–444 (2012).
18. Liu, M., An, D., Hou, L., Yu, S. & Zhu, Y. Zero valent iron particles impregnated zeolite X composites for adsorption of tetracycline in aquatic environment. *RSC Adv.* **5**, 103480–103487 (2015).
19. Alam, S. *et al.* Comparative study on the magnetic properties of iron oxide nanoparticles loaded onmesoporous silica and carbon materials with different structure. *Microporous Mesoporous Mater.* **121**, 178–184 (2009).
20. Alam, S., Anand, C., Ariga, K., Mori, T. & Vinu, A. Unusual magnetic properties of size-controlled iron oxide nanoparticles grown in a nanoporous matrix with tunable pores. *Angew. Chem.* **121**, 7494–7497 (2009).
21. Yihan, W. *et al.* Environmental remediation of heavy metal ions by novel-nanomaterials: a review. *Environ. Pollut.* **246**, 608–620 (2019).
22. Guo, Y. *et al.* Synthesis of chitosan-functionalized MCM-41-A and its performance in Pb(II) removal from synthetic water. *J. Taiwan Inst. Chem. Eng.* **71**, 537–545 (2017).
23. Lin, K. *et al.* Direct room-temperature synthesis of methyl-functionalized Ti-MCM-41 nanoparticles and their catalytic performance in epoxidation. *J. Catal.* **263**, 75–82 (2009).
24. Fu, Y. *et al.* High efficient removal of tetracycline from solution by degradation and flocculation with nanoscale zerovalent iron. *Chem. Eng. J.* **270**, 631–640 (2015).
25. Zhang, S. *et al.* A novel biochar supported CMC stabilized nano-zero-valent iron composite for hexavalent chromium removal from water. *Chemosphere* **217**, 686–694. https://doi.org/10.1016/j.chemosphere.2018.11.040 (2019).
26. Liu, M., Xi, B., Hou, L. & Shuli, Yu. Magnetic multi-functional nano-fly ash-derived zeolite composites for environmental applications. *J. Mater. Chem. A* **1**, 12617–12626 (2013).
27. Yi, Yu., Xiong, G., Li, C. & Xiao, F.-S. Characterization of iron atoms in the framework of MFI-type zeolites by UV resonance Raman spectroscopy. *J. Catal.* **194**, 487–490 (2000).
28. Jouinia, H. *et al.* Characterization and NH3-SCR reactivity of Cu-Fe-ZSM-5 catalysts prepared by solid state ion exchange: the metal exchange order effect. *Microporous Mesoporous Mater.* **260**, 217–226 (2018).
29. Santhosh Kumar, M., Schwidde, M., Grünert, W. & Brückner, A. On the nature of different iron sites and their catalytic role in Fe-ZSM-5DeNOx catalysts: new insights by a combined EPR and UV/VISspectroscopic approach. *J. Catal.* **227**, 384–397 (2004).
30. Wang, L. *et al.* Effects of annealing temperature on structure and magnetic properties of Co Al0.2Fe1.8O4/SiO2 nanocomposites. *J. Magnet. Magn. Mater.* **324**, 4200–4203 (2012).
31. Xiao, J. *et al.* Fe-doped ZnO nanoparticles: the oxidation number and local charge on iron, studied by 57Fe Mçßbauer spectroscopy and DFT calculations. *Chem. Eur. J.* **19**, 3287–3291 (2013).
32. Ratnayake, S. *et al.* A novel radiation-induced grafting methodology to synthesize stable zerovalent iron nanoparticles at ambient atmospheric conditions. *Colloid Polym. Sci.* **294**, 1557–1569 (2016).
33. Wang, Y., Yu, L., Wang, R., Wang, Y. & Zhang, X. A novel cellulose hydrogel coating with nanoscale Fe0 for Cr(VI) adsorption and reduction. *Sci. Total Environ.* **726**, 138625. https://doi.org/10.1016/j.scitotenv.2020.138625 (2020).
34. Mortazavian, S., An, H., Chun, D. & Moon, J. Activated carbon impregnated by zero-valent iron nanoparticles (AC/nZVI) optimized for simultaneous adsorption and reduction of aqueous hexavalent chromium: material characterizations and kinetic studies. *Chem. Eng.* **353**, 781–795 (2018).
35. Hanay, Ö., Yıldız, B. & Aslan, S. Removal of tetracycline and oxytetracycline by microscale zerovalent iron and formation of transformation products. *Environ. Sci. Pollut. Res.* **21**, 3774–3782 (2014).
36. Zhang, W., Qian, L., Ouyang, Da., Yun Chen, Lu. & Han, M. C. Effective removal of Cr(VI) by attapulgite-supported nanoscale zero-valent iron from aqueous solution: enhanced adsorption and crystallization. *Chemosphere* **221**, 683–692 (2019).
37. An, W. H., Xiao, H. & Yu, M. Adsorptive removal of trace oxytetracycline from water by acid-modified zeolite: influencing factors. *Water Sci. Technol.* **68**, 2473–2478 (2013).
38. Zhang, Z. Y., Lan, H. C. & Liu, H. J. Iron-incorporated mesoporous silica for enhanced adsorption of tetracycline in aqueous solution. *RSC Adv.* **5**, 1–7 (2015).
39. Zhao, Y., Tong, F. & Gu, X. Insights into tetracyclineadsorption onto goethite: experiments and modeling. *Sci. Total Environ.* **470**, 19–25 (2014).
40. Eugeniaparolo, M., Marcelo, J. A. & Gisela, R. P. Influence of Ca^{2+} on tetracycline adsorption on montmorillonite. *J. Colloid Interfaces* **368**, 420–426 (2012).
41. Maximiliano, B. & Marcelo, A. Biotemplated synthesis of mesoporous silica for doxycycline removal Effect of pH, temperature, ionic strength and Ca^{2+} concentration on the adsorption behaviour. *Micro Meso Mater.* **225**, 534–542 (2016).
42. Jin, T., Liu, Y. & Dong, Y. H. Adsorption of sulfamonomethoxine antibiotics to cucurbit uril-anchored silica gel: effect of aqueous solution chemistry. *Desalin. Water Treat.* **56**, 552–563 (2014).

43. Jiayan, Wu., Wang, Y., Zixuan, Wu., Gao, Ya. & Li, X. Adsorption properties and mechanism of sepiolite modified by anionic and cationic surfactants on oxytetracycline from aqueous solutions. *Sci. Total Environ.* **708**, 134409. https://doi.org/10.1016/j.scitotenv.2019.134409 (2020).
44. Kan, Y., Yue, Q., Li, D., Yuwei, Wu. & Gao, B. Preparation and characterization of activated carbons from waste tea by H_3PO_4 activation in different atmospheres for oxytetracycline removal. *J. Taiwan Inst. Chem. E* **71**, 494–500 (2017).
45. Martucci, A. *et al.* Adsorption and reaction of sulfachloropyridazine sulfonamide antibiotic on a high silica mordenite: a structural and spectroscopic combined study. *Micro Meso Mater.* **170**, 274–286 (2013).
46. Roik Nadiia, V., Belyakova Lyudmila, A. & Dziazko, M. O. Adsorption of antitumor antibiotic doxorubicin on MCM-41-type silica surface. *Adsorpt. Sci. Technol.* **35**, 86–101 (2017).
47. Ji, L. *et al.* Adsorption of tetracycline on single-walled and multi-walled carbon nanotubes as affected by aqueous solution chemistry. *Environ. Toxicol. Chem.* **29**, 2713–2719 (2010).
48. Liang, G. *et al.* Effective removal of tetracycline from aqueous solution by organic acid-coated magnetic nanoparticles. *J. Nanosci. Nanotechnol.* **16**, 2218–2226 (2016).
49. Tianding, Hu. *et al.* Porous structured MIL-101 synthesized with different mineralizers for adsorptive removal of oxytetracycline from aqueous solution. *RSC Adv.* **6**, 73741–73747 (2016).
50. Song, X. *et al.* Adsorption mechanisms and the effect of oxytetracycline on activated sludge. *Biores. Technol.* **151**, 428–431 (2014).
51. Ocampo-Pérez, R., Leyva-Ramos, R., Rivera-Utrilla, J., Flores Cano, J. V. & Sánchez-Polo, M. Modeling adsorption rate of tetracyclines on activated carbons from aqueous phase. *Chem. Eng. Res. Des.* **104**, 579–588 (2015).
52. Zhang, Yu. *et al.* Molecular insights into the ph-dependent adsorption and removal of ionizable antibiotic oxytetracycline by adsorbent cyclodextrin polymers. *PLoS ONE* **9**, 1–11 (2014).
53. Patrykoleszczuk, B. Influence of anionic, cationic and nonionic surfactants on adsorption and desorption of oxytetracycline by ultrasonically treated and non-treated multiwalled carbon nanotubes. *Chemosphere* **85**, 1312–1317 (2011).
54. Wang, Y., Zhang, Y., Hou, C., He, X. & Liu, M. Preparation of a novel TETA functionalized magnetic PGMA nano-absorbent by ATRP method and used for highly effective adsorption of Hg(II). *J. Taiwan Inst. Chem. E* **58**, 283–289 (2016).

Acknowledgements

This work was supported by Xi'an University of Science and Technology and Beijing advanced innovation Center for Future Urban Design of Beijing University of Civil Engineering and Architecture (No. 2017032512).

Author contributions

Y.G.: Writing-Original Draft, Methodology, Validation. B.C.: Formal analysis, Data curation, Writing—Review & Editing. Y.Z.: Resources, Supervision. T.Y.: Conceptualization, Supervision.

Competing interests

The authors declare no competing interests.

Additional information

Supplementary Information The online version contains supplementary material available at https://doi.org/10.1038/s41598-021-81928-8.

Correspondence and requests for materials should be addressed to B.C. or T.Y.

Reprints and permissions information is available at www.nature.com/reprints.

Publisher's note Springer Nature remains neutral with regard to jurisdictional claims in published maps and institutional affiliations.

Open Access This article is licensed under a Creative Commons Attribution 4.0 International License, which permits use, sharing, adaptation, distribution and reproduction in any medium or format, as long as you give appropriate credit to the original author(s) and the source, provide a link to the Creative Commons licence, and indicate if changes were made. The images or other third party material in this article are included in the article's Creative Commons licence, unless indicated otherwise in a credit line to the material. If material is not included in the article's Creative Commons licence and your intended use is not permitted by statutory regulation or exceeds the permitted use, you will need to obtain permission directly from the copyright holder. To view a copy of this licence, visit http://creativecommons.org/licenses/by/4.0/.

© The Author(s) 2021